International Journal of Applied Earth Observations and Geoinformation 115 (2022) 103123

Contents lists available at ScienceDirect

International Journal of Applied Earth Observations and Geoinformation

journal homepage: www.elsevier.com/locate/jag

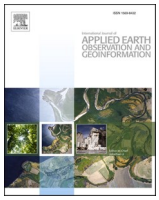

Mapping Lower Saxony's salt marshes using temporal metrics of multi-sensor satellite data

Kim-Jana Stückemann *, Björn Waske

Osnabrück University, Institute of Computer Science, Remote Sensing and Digital Image Analysis, Wachsbleiche 27, 49090 Osnabrück, Germany

ARTICLE INFO

Keywords:
Salt marshes
Spectral-temporal metrics
Multi-sensor
Sentinel-2
Sentinel-1
Landsat 8

ABSTRACT

Salt marshes act as an important natural buffer in terms of coastal protection in the light of the rising sea level. Due to weather events like extreme storms the extent of salt marshes changes. Hence, it is of great importance to regularly monitor these changes, especially for managing interventions and reporting their ecological status in the frame of environmental policies, like Natura 2000. In this study, the potential of freely available sallite imagery is investigated and a methodological approach suggested to map superior salt marsh types (pioneer zone, lower and upper salt marshes) for supporting regular monitoring compliances. Therefore, (spectral-)temporal metrics of optical Sentinel-2 (S2) and Landsat 8 as well as SAR Sentinel-1 were calculated and used in different classification setups. The classifications were performed using a basic Random Forest classifier. A detailed accuracy assessment shows the impact of different datasets on the overall accuracy. The best result was achieved using S2 data, which led to an overall accuracy of 90.3 %. The combination of optical and SAR data, on the other hand, did not increase the classification accuracy. Overall, the freely available datasets and the proposed method proof useful and are considered well suited for monitoring salt marshes.

1. Introduction

Salt marshes as part of global wetlands occur across the coasts of all continents and in all climate zones. As natural wave-breaker, salt marshes play an important role in the protection of coastal regions (Gedan et al., 2011; Davy et al., 2009). In face of the sea-level rise, they are exposed to extensive changes (Schuerch et al., 2018). Globally, a loss of 50 % of salt marshes is reported by Gedan et al. (2011). The consequences of climate change further promote their degradation as hydrological regimes change and marsh areas get reclaimed (Silliman et al., 2009). This study focusses on the salt marshes of Germany's federate state Lower Saxony.

1.1. Salt marshes in Lower Saxony, Germany

During the 20th century, the salt marsh extent in Lower Saxony declined due to the reclamation of land for agriculture and artificial coastal protection. Recent observations, however, show an expansion of salt marshes (Esselink et al., 2009; Esselink et al., 2019). Thus, in 2004, they occupied a region of 9.660 ha (Esselink et al., 2019). The region is an important breeding and roosting place and is, for this reason, listed under the European environmental policies *Flora-Fauna-Habitat (FFH)* and the *Birds Directive*, as part of the World Heritage – natural site Wadden Sea. According to *Natura 2000*, European countries are obliged to report the status of FFH regions every-six years (European Commission 2008). To date, in Lower Saxony, the reporting is based on field mapping complemented by visual interpretation of airborne imagery. As a consequence, this method is associated with several disadvantages, which are: the dependency on favorable weather conditions for airborne image acquisition, the subjective visual interpretation of image data, the dependence on the mapper's experience and lastly, the time and labour intensity involved. To address this, today's availability of free satellite imagery and processing tools fosters its use for automated monitoring and eventually, the operational reporting commitment bound to international environmental treaties.

1.2. Current state of research: Remote sensing of salt marshes

With the start of the Copernicus Mission and the launch of its first satellite Sentinel-1A in 2014, freely available SAR imagery at high spatial resolution of 10 m is provided, followed by the optical Sentinel-2 mission in 2015. Additionally, the opening up of the Landsat archive in

* Corresponding author.
E-mail address: kimjana.stueckemann@uni-osnabrueck.de (K.-J. Stückemann).

https://doi.org/10.1016/j.jag.2022.103123
Received 30 August 2022; Received in revised form 18 November 2022; Accepted 20 November 2022
Available online 24 November 2022

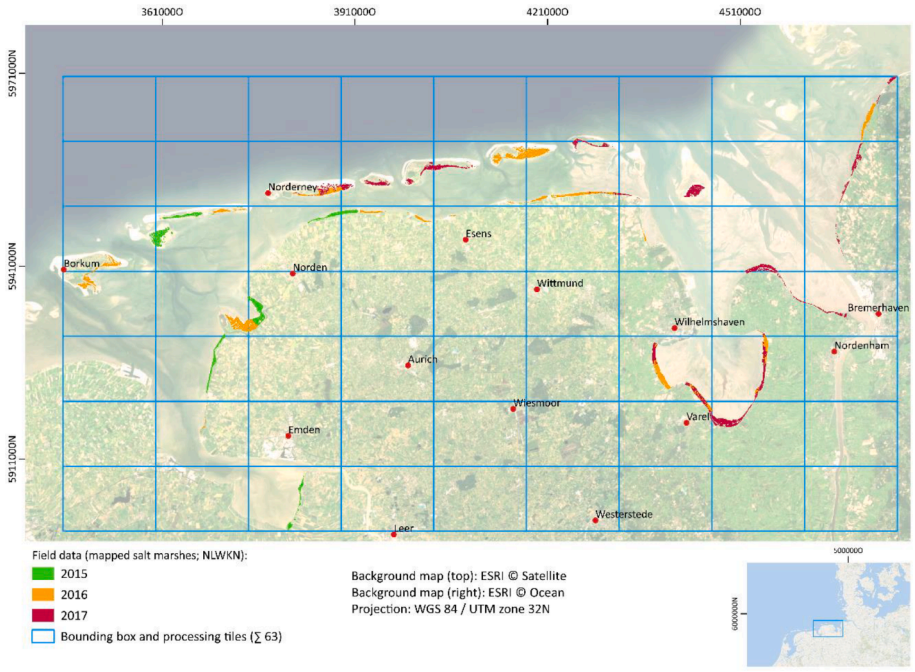

Fig. 1. Overview of the study area including field data. The green, yellow and red areas visualise the salt marsh extent mapped in the field by NLWKN in 2015, 2016 and 2017, respectively. The blue grid represents the 63 processing units based on the bounding box (outer box and thumb map) of the salt marsh extent.

2008 fosters its use for long-time change analysis of the Earth's surface. The value of these freely available satellite image datasets for mapping salt marshes at different levels is expounded in the following mentioned studies. Zhang et al. (2021) mapped the distribution of salt marsh species using Sentinel-1 and Sentinel-2 based on spectral, spatial, and temporal features. The authors show that a combination of optical and SAR data leads to better classification results than using the single datasets for classification. The authors showed that the combined dataset of spectral, temporal and spatial features leads the best result and is capable of differentiating among three salt marsh types and mudflats. Neither optical nor SAR data alone provides sufficient information to distinguish among the classes. Hu et al. (2021) used annual Sentinel-1 metrics and decision tree (DT) classifiers to map four salt marsh plant species in China and found the annual mean to be more stable using statistical measures instead of seasonal metrics, therewith obtaining an overall accuracy (OA) of 87.86 %. The authors found that a large number of training samples and high resolution, multi-polarization SAR data increases the accuracy. Li et al. (2021) conducted a classification of superior salt marsh categories (low and high marsh) in South Carolina and attained an OA of 95 % for low marsh and 93 % for high marsh using nine Sentinel-2 bands and the NDVI of 20 images collected over one year in a deep learning approach. Sun et al. (2018) analysed changes in salt marsh vegetation communities using flexible monthly NDVI time-series based on multi-temporal Landsat 5 and 7 data using DTs. Therewith, they achieved an OA of 89.8 % compared to using single multi-spectral images (avg. OA of 79.1 %). Sun et al. (2021) used a pixel-differential time series of Sentinel-2 NDVI of 30 scenes collected over one year to map six different plant species of salt marshes. With their Random Forest classification based on GPS, UAV and Google Earth data, they achieved an average overall accuracy of 81.5 %. Zeng et al. (2022) mapped salt marshes on species level using a pixel- and phenology-based algorithm with accuracies around 90 %. Common challenges that were highlighted by most of the cited authors (Li et al., 2021; Sun et al., 2021; Zeng et al., 2022) are the frequent cloud cover leading to a limited availability of optical data, the heterogeneous distribution of plant species among the salt marsh categories lower and upper marsh as well as the influence of the tide on the spectral reflectance and the SAR signal. The current state of research shows that up to date, no study exists that uses temporal metrics of optical and SAR data for mapping salt marshes on the superior level of the pioneer zone, lower and upper salt marsh. Additionally, this paper provides a systematic comparison of free satellite data for mapping salt marshes, which is the preferred data for operational monitoring.

1.3. Study objective

Our study has three aims: 1) Assessing the general quality of salt marsh mapping using freely available satellite imagery to support regular monitoring compliances; 2) Comparing the classification accuracy of Sentinel-2 to Landsat 8; and 3) Assessing the added value of Sentinel-1 imagery to the mapping accuracy. To address our aims, we chose Sentinel-2 and Landsat 8 as freely available image products with the highest spatial resolution and comparable spectral resolution (Mandanici and Bitelli, 2016), allowing for completion if data is limited (Wang et al., 2017; Cao and Tzortziou, 2021). Additionally, Sentinel-1 was included as SAR data adds valuable complementary information to vegetation mapping (Joshi et al., 2016; Muro et al., 2020). The conducted classifications were based on (spectral-)temporal metrics, condensing multi-temporal spectral information in statistical measures, e.g., mean. Based on the chosen datasets, we defined seven classification setups by combining the datasets to conduct a supervised classification using the widely known and used Random Forest (RF) classification approach.

2. Study area and materials

2.1. Study area

The study area encompasses the salt marshes of the entire coastline of Lower Saxony, bordering the German Wadden Sea (North Sea; Fig. 1). Besides the mainland coast, the study area encompasses the East Frisian Islands (from West to East: Borkum, Memmert, Juist, Norderney, Baltrum, Langeoog, Spiekeroog, Wangerooge; Fig. 1).

The study area succumbs the influence of semidiurnal tides. The mean high water measured at Norderney (Riffgat) is 6.23 m tide gauge zero (Bundesamt für Seeschifffahrt und Hydrographie, 2022). The salt

Table 1
Overview of the salt marsh vegetation types pooled to three superior categories used in the classifications. The TMAP codes are given in the dataset provided by NLWKN and TMAP types are taken from Common Wadden Sea Secretariat (2017).

Pioneer zone		Lower salt marsh		Upper salt marsh	
TMAP Code	TMAP type	TMAP Code	TMAP type	TMAP Code	TMAP type
S.1.1	*Spartina anglica*	S.2	Low marsh	S.3	High marsh
S.1.2	*Salicornia*	S.2.0	Low marsh, unspecific	S.3.0	High marsh, unspecific
		S.2.1	*Puccinellia maritima / Limonium vulgare*	S.3.1	*Limonium vulgare / Juncus gerardii*
		S.2.2	*Puccinellia maritima*	S.3.2	*Juncus gerardii*
		S.2.3	*Aster tripolium*	S.3.3	*Festuca rubra*
		S.2.4	*Puccinellia maritima / Atriplex portulacoides*	S.3.4	*Atriplex portulacoides/ Artemisia maritima*
				S.3.5	*Artemisia maritima / Festuca rubra*
				S.3.6	*Juncus maritimus*
				S.3.7	*Elymus athericus*
				S.3.8	*Carex extensa*
				S.3.9	*Atriplex prostrata / A. littoralis*
				S.3.10	*Agrostis stolonifera / Trifolium fragiferum*
				S.3.12	*Ononis spinosa / Carex distans*
				S.3.13	*Elymus repens*
				S.3.14	Ruderal salt marsh areas

marshes are characterised by 23 different vegetation types (Table 1), which are grouped into three categories in this study (see 2.2.). When sediments accumulate and first plants colonise, the pioneer zone develops (Fig. 2). This is the first stage of a developing salt marsh, mainly dominated by the species *Spartina anglica*. The pioneer zone is regularly flooded at high tide. After a few years, the pioneer zone transitions into a lower salt marsh. Lower salt marshes are characterised by a small variety of vegetation types, dominated by *Puccinellia maritima*. This zone is still flooded regularly. Upper salt marshes then develop from lower salt marshes and are characterised by even more diverse vegetation species (Table 1) and less frequent flooding.

2.2. Field data

The field data was provided by Lower Saxony Water Management, Coastal Defense and Nature Agency (*German:* "Niedersächsischer Landesbetrieb für Wasserwirtschaft, Küsten- und Naturschutz", NLWKN). The dataset prescribed the geographic extent for this study (see bounding box, Fig. 1). Fig. 1 shows in which years which parts of the study site were mapped in the field. The field mapping was done according to the Trilateral Monitoring and Assessment Programme (TMAP). TMAP encompasses a typology for the coastal vegetation in the Wadden Sea region across the Netherlands, Germany, and Denmark. For this study, the TMAP vegetation types were grouped into three superior categories: 1) pioneer zone, 2) lower salt marsh, and 3) upper salt marsh (Table 1). In 2015, the field mapping was started in the West of the study area and was continued towards the East in the following year. The mapping was completed in 2017 with the salt marshes in the centre and East of the study area.

The field data provided by NLWKN (see 2.2.) was used for generating the reference data for the classification. Polygons for each salt marsh class were collected in the centre of connected salt marsh areas, therewith avoiding the inclusion of mixed pixels along boundaries. In preparation for the training of the RF classifiers (see 3.2.) and the accuracy assessment (see 3.3.), this reference dataset was divided into a training

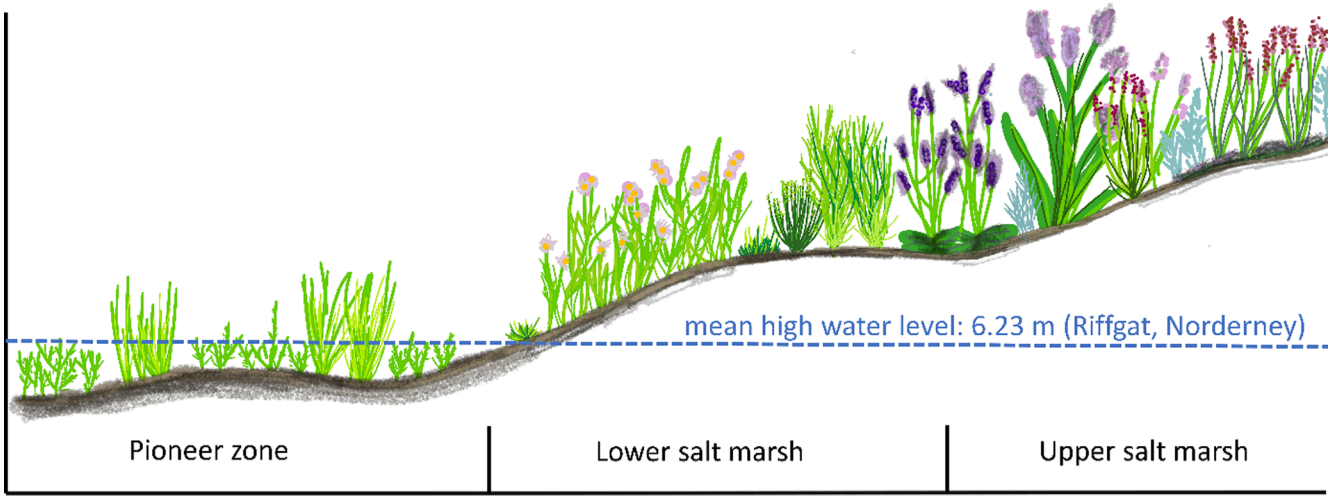

Fig. 2. Salt marsh profile showing the zonation of each superior salt marsh category (pioneer zone, lower salt marsh, and upper salt marsh). The mean high water level is 6.23 m tide gauge zero, measured at Riffgat (Norderney).

Table 2
Area (in ha) and estimated count of pixels based on a spatial resolution of 10 m.

	Pioneer zone		Lower salt marsh		Upper salt marsh	
	Area in ha	Estimated count of pixels	Area in ha	Estimated count of pixels	Area in ha	Estimated count of pixels
Training	42.45	4245	48.29	4831	41.41	4143
Validation	35.92	3597	27.84	2786	34.18	3420

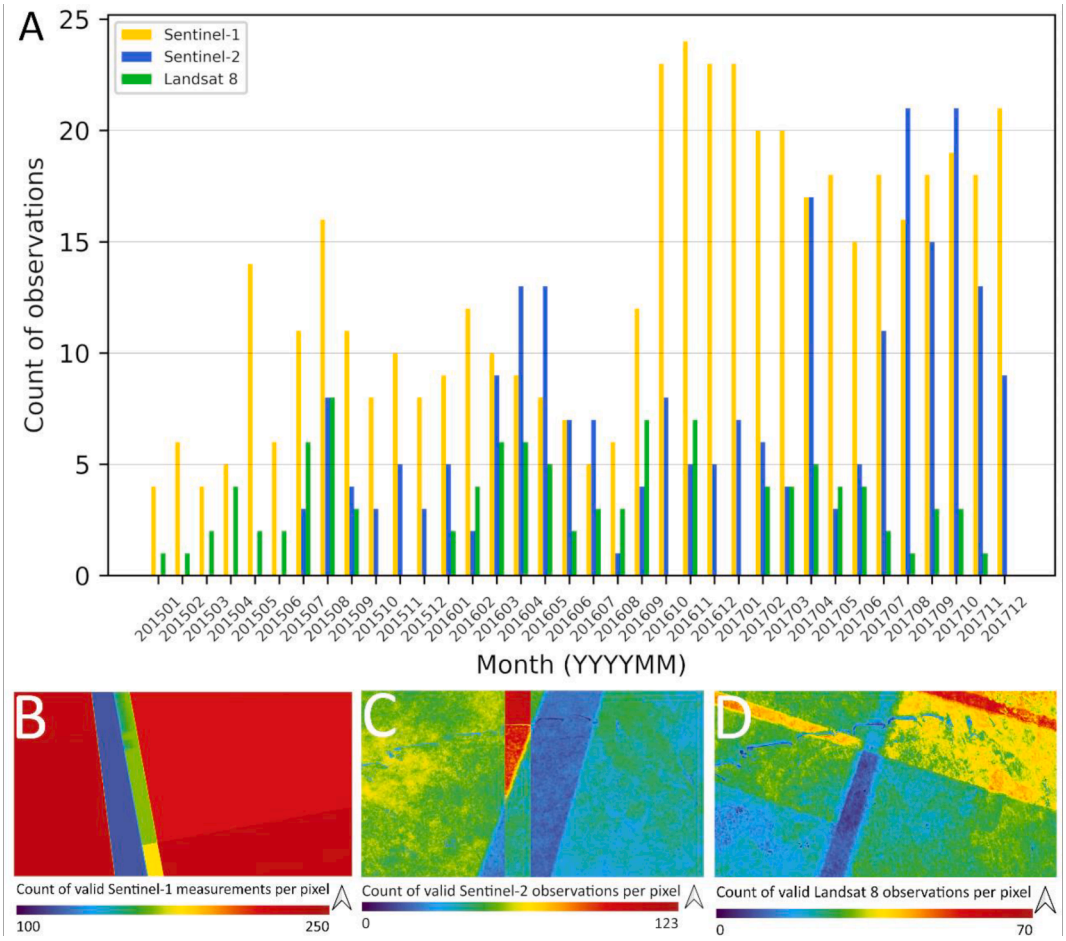

Fig. 3. Count of valid observations per month (A) of the observation period (01/01/2015 – 31/12/2017). Sharp increases in available datasets can be explained by the launch of the respective twin satellite of Sentinel-1 and Sentinel-2. The maps B-D show the per pixel count of valid Sentinel-1 measurements and the valid Sentinel-2 and Landsat 8 observations (cloud cover ≤ 50 %), respectively.

(60 %) and a spatially independent validation dataset (40 %) using a stratified random selection function. Table 2 gives an overview of the area proportions of the salt marsh classes.

2.3. Satellite data and pre-processing

The field mapping period of three years (see 2.2.) predetermined the period over which the satellite data was acquired. We decided to use Sentinel-2 for reasons of its high spatial resolution to map small scale salt marshes and the high temporal resolution with a repetition rate of five days. The combined use of optical and SAR data has shown to be more powerful and accurate in LULC classifications than mono-sensor approaches (Joshi et al., 2016; Ienco et al., 2019). Thus, we included Sentinel-1. Landsat 8 data was chosen for complementing reasons. Of each satellite data type, all available products over the field mapping period 01/01/2015 to 31/12/2017 were used: 474 Sentinel-1, 237 Sentinel-2 and 105 Landsat 8 images were available. The search for optical data was constrained with a cloud cover of max. 50 %. The respective amount of datasets per month is visualised in Fig. 3.

Sentinel-1 (S1) is a C-band SAR constellation with dual-band cross-polarization (VV, VH). We only used S1 data measured in the ascending orbit as only a few datasets were available in descending orbit. The data was obtained from Google Earth Engine (GEE). Therein, S1 data is provided ready-to-use, including thermal noise removal, radiometric calibration, terrain correction and the conversion to decibels via log scaling. For our analysis, we converted the S1 data back to linear scale (see Fig. 4). The spatial resolution is 10 m. Besides the original VV and VH band, three SAR indices were calculated according to Hu et al. (2021; Eqs. (1) - (3)) and completed by the common SAR band ratio (Eq. (4), Veloso et al., 2017). Hu et al. (2021) showed that the listed SAR indices add value for mapping coastal salt marshes. Veloso et al. (2017) proofed the suitability of the SAR ratio in reducing the double-bounce effect and thus conclude it to be more stable than the VV or VH backscatter.

$$SAR_{sum} = VV + VH \quad (1)$$

$$SAR_{diff} = VH - VV \quad (2)$$

$$SAR_{NDVI} = (VV - VH) / (VV + VH) \quad (3)$$

$$SAR_{ratio} = VH / VV \quad (4)$$

Sentinel-2 (S2) Level-1C products were downloaded from the German Copernicus Data and Exploitation Platform (CODE-DE). The atmospheric correction was conducted using the standalone version of sen2cor. Further pre-processing was implemented in Python 3.7 (Van Rossum and Drake, 2009) using the libraries GDAL/OGR 3.1.3 (GDAL/OGR contributors, 2021), NumPy 1.20.1 (Harris et al., 2020) and Scikit-learn 0.21.0 (Pedregosa et al., 2011) in Jupyter Notebooks. We included all bands except for B1, B9 and B10, as these are basically used for the atmospheric correction and would not contribute to vegetation differentiation, and B8a due to its lower spatial resolution compared to B8. The original bands in 20 m spatial resolution were resampled to 10 m using the nearest neighbour method. Subsequently, clouds and shadows were masked using the scene classification (SCL), which is a byproduct

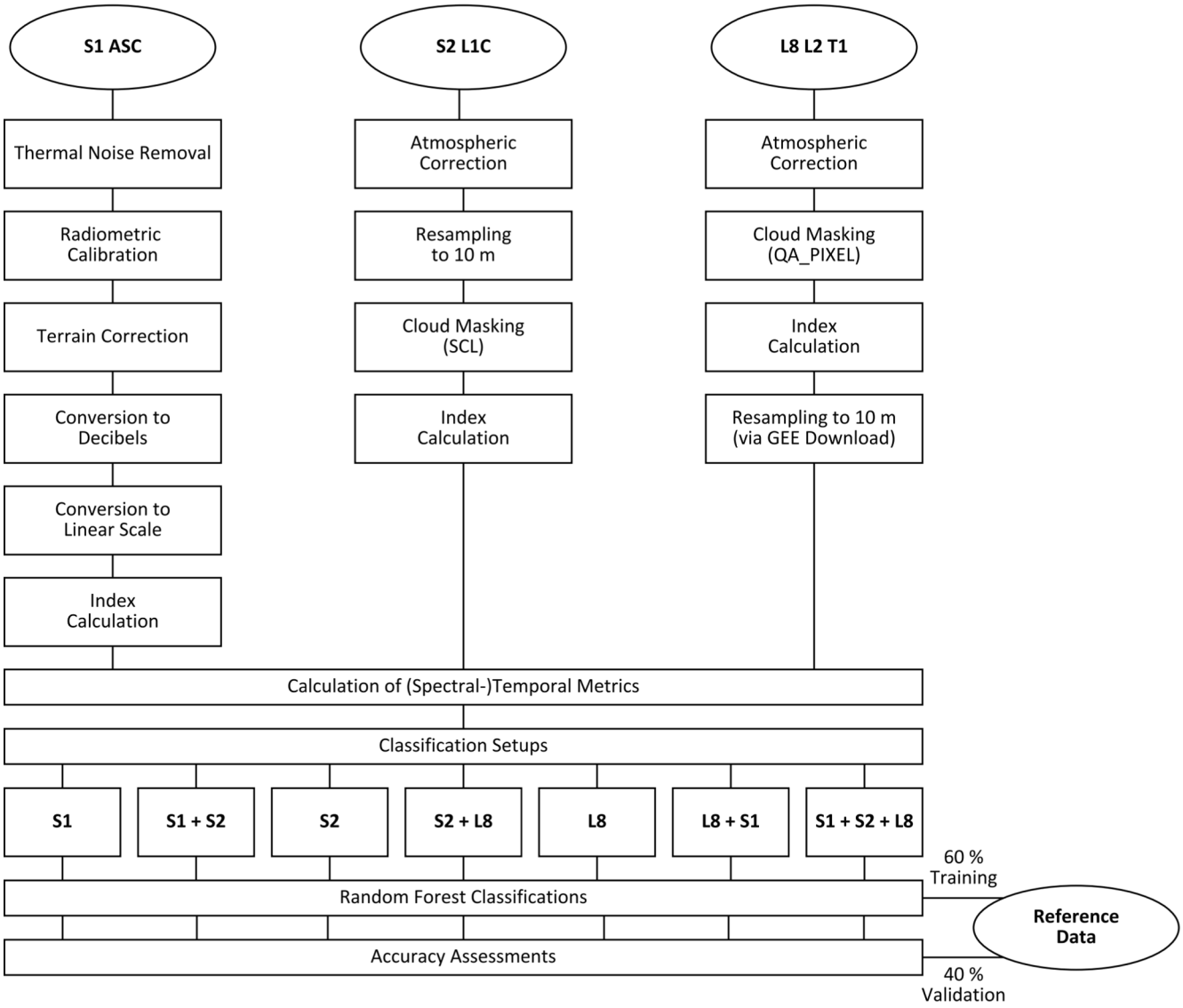

Fig. 4. Processing workflow.

of the atmospheric correction. The SCL values 3 (cloud shadows), 8 (cloud of medium probability), 9 (cloud of high probability) and 10 (thin cirrus) (ESA 2021) were masked. Following this approach for masking is straight forward, but misses the detection of some clouds and shadows, especially on the edges. As the classification was based on spectral-temporal metrics, of which most allow outliers to have minor influence, we disregarded an improvement. To handle the processing effort of the metric calculations, 63 smaller patches were created based on the bounding box of the mapped salt marshes (Fig. 1). Fig. 3B-D show the per pixel count of valid Sentinel-1, Sentinel-2 and Landsat 8 measurements (observations), respectively.

Landsat 8 (L8; Level 2, Collection 2, Tier 1) data was obtained and pre-processed in GEE. Products of this collection are processed to orthorectified and atmospherically corrected surface reflectance. Clouds and shadows were masked using the QA_PIXEL band, which represents the pixel quality derived by the CFMASK algorithm (values 1–3 represent clouds and 4 shadows). The data was downloaded from GEE with 10 m spatial resolution to match the Sentinel data. To complete the pre-processing, two indices were calculated: the Normalized Difference Vegetation Index (NDVI; Tucker, 1979, Eq. (5), using B5 (NIR) and B4 (red) of L8 as well as B8 (NIR) and B4 (red) of S2) and the Tidal Marsh Inundation Index (TMII; O'Connell et al., 2017; Eq. (8)). Beneath the Normalized Difference Water Index (NDWI) calculated based on the green and SWIR2 band (McFeeters, 1996; Eq. (6)), the TMII requires the NDWI calculated of NIR and SWIR1 (Gao, 1996; Eq. (7)) to be monthly averaged, resulting in a rolling mean (O'Connell et al., 2017). The rolling mean is calculated for each month of the observation period. Campbell and Wang (2020) demonstrated a successful filtering of Landsat data based on the TMII. We adapted it to L8 (green: 555 nm, SWIR1: 1240 nm, SWIR2: 1640 nm) and S2 (green: 559 nm, SWIR1: 1613 nm, SWIR2: 2202 nm) by selecting the corresponding wavelengths.

$$NDVI = (NIR - Red)/(NIR + Red) \tag{5}$$

$$NDWI_{Green,SWIR2} = (Green - SWIR2)/(Green + SWIR2) \tag{6}$$

$$NDWI_{NIR,SWIR1} = (NIR - SWIR1)/(NIR + SWIR1) \tag{7}$$

$$TMII = 1 - \frac{1}{e^{0.3+16.6*NDWI_{Green,SWIR2}-25.2*rollingMean(NDWI_{NIR,SWIR1})}} \tag{8}$$

Table 3
Accuracy assessment of the seven RF classifications using a CI of 95 %.

Classification setup		PA	UA	OA
1	**Sentinel-2**			
	Pioneer zone	92.71 ± 0.57	90.35 ± 1.00	90.31 ± 0.59
	Lower salt marsh	70.31 ± 2.05	78.36 ± 1.46	
	Upper salt marsh	97.13 ± 0.38	95.50 ± 0.70	
2	**Sentinel-1 + Sentinel-2**			
	Pioneer zone	93.21 ± 0.51	90.83 ± 0.99	90.18 ± 0.60
	Lower salt marsh	69.42 ± 2.12	76.82 ± 1.48	
	Upper salt marsh	96.61 ± 0.41	95.47 ± 0.70	
3	**Sentinel-1**			
	Pioneer zone	86.04 ± 0.69	64.99 ± 1.65	63.08 ± 1.16
	Lower salt marsh	28.02 ± 1.40	44.63 ± 1.53	
	Upper salt marsh	49.88 ± 1.60	68.68 ± 1.81	
4	**Landsat 8**			
	Pioneer zone	87.00 ± 0.89	84.41 ± 1.19	81.57 ± 0.79
	Lower salt marsh	75.39 ± 1.41	69.40 ± 1.62	
	Upper salt marsh	79.63 ± 1.37	95.09 ± 0.76	
5	**Landsat 8 + Sentinel-2**			
	Pioneer zone	88.04 ± 0.85	87.75 ± 1.09	86.10 ± 0.71
	Lower salt marsh	80.58 ± 1.35	76.81 ± 1.52	
	Upper salt marsh	89.67 ± 1.18	96.65 ± 0.62	
6	**Landsat 8 + Sentinel-1**			
	Pioneer zone	87.29 ± 0.87	86.57 ± 1.13	82.98 ± 0.78
	Lower salt marsh	78.58 ± 1.38	72.29 ± 1.58	
	Upper salt marsh	80.08 ± 1.55	94.60 ± 0.78	
7	**Sentinel-1 + Sentinel-2 + Landsat 8**			
	Pioneer zone	87.41 ± 0.90	88.06 ± 1.08	85.53 ± 0.75
	Lower salt marsh	82.51 ± 1.28	77.33 ± 1.50	
	Upper salt marsh	86.29 ± 1.55	96.31 ± 0.64	

3. Methodology

3.1. (Spectral-)Temporal metrics

Spectral-temporal metrics condense pixel-wise spectral reflectance measured over a predefined period into statistical metrics. Common calculated metrics are the minimum, maximum, 10th, 25th, 50th, 75th and 90th percentiles, the interquartile range (IQR), mean, median and standard deviation, whereby these are either calculated based on the original bands or on any type of band transformation, e.g., NDVI (Muro et al., 2020; Dara et al., 2020; Pflugmacher et al., 2019; Potapov et al., 2015; Rufin et al., 2015). This approach allows the generation of cloud-free composites, especially for larger investigated periods and wide areas. Moreover, the data volume can be reduced while extracting and preserving important spectral-temporal information. Initially, this approach became useful with the opening of the Landsat archive in 2008. Now, with the availability of frequent Sentinel-2 observations, spectral-temporal metrics become more popular. The term was introduced by Müller et al. in 2015, whereby the concept was already implemented by Griffiths et al. (2013) and Hansen (2013). While spectral-temporal metrics were mainly used in the context of multi-spectral data and the generation of cloud-free composites, temporal metrics qwre also used in a variety of SAR-based LULC studies (Bruzzone et al., 2004; Rüetschi et al., 2019; Carrasco et al., 2019). In the context of salt marsh mapping, so far, only one study used a temporal metric of SAR data (Hu et al., 2021; see 1.2). The kind of spectral-temporal metric used in each study varies with the dataset and the application. In our study, we calculated pixel-based the following temporal metrics of S1 data over the whole period (01/01/2015 – 31/12/2017): median, variance, 1st quartile (Q_{25}), 3rd quartile (Q_{75}) and IQR. Based on the 63 processing units, the data was downloaded from GEE for the classifications on a local machine. For S2 and L8, the following spectral-temporal metrics were calculated over the same period: mean, median, variance, 10th percentile (Q_{10}), Q_{25}, Q_{75}, 90th percentile (Q_{90}) and IQR. The calculation of the metrics of S2 as well as the data export of L8 was conducted based on the 63 processing tiles shown in Fig. 1. In all, the calculation of (spectral-)temporal features resulted in 88 S2, 64 L8 and 30 S1 features.

3.2. Data fusion and Random Forest classification

This study aims at assessing the potential of freely available satellite imagery for salt marsh mapping. Our aim was to map the three superior salt marsh classes pioneer zone, lower and upper salt marsh and investigate the suitability of mono-sensor and fused datasets in detail. In general, methods of data fusion can be grouped into three categories, depending on the level at which the fusion is performed: 1) pixel-level fusion (data fusion); 2) feature fusion; and 3) decision fusion. Although the classification accuracy may increase due to complex fusion strategies (Waske and Benediktsson, 2007), the majority of the studies were based on a simple pixel-based data fusion (Joshi et al., 2016; Zhang et al. 2021). Due to the simplicity, the pixel-based fusion technique seems also interesting for a regular large scale monitoring and was therefore used in this study. Consequently, seven different classification setups were built by merging the respective features into one image stack for individual classifications (Fig. 4). Besides three mono-sensor classification setups, four combined ones were built. S2 and S1 were fused to assess the added value of SAR data. S2 was complemented by L8 data to evaluate if a denser time series of optical data allows more accurate classifications. Lastly, the combination of L8 and S1 as well as L8, S1 and S2 were classified. All classifications were performed using a Random Forest classifier, which was initially proposed by Breiman (2001). RFs are easy to parametrise and are characterized by a relatively small computation time (Waske et al., 2012). Moreover, RFs outperform other algorithms in terms of mapping accuracy, particularly, when dealing with multi-sensor and multi-temporal SAR data or small training sample sets (Waske and Benediktsson, 2007). In the last decades, RFs were used in a wide range of remote sensing image classifications (Belgiu and Drăguţ, 2016), which includes as well the mapping of salt marshes (Sun et al., 2021; Zhang et al., 2021). A basic parametrisation (500 trees, max. number of features being the square root of all features) was chosen, which yielded good results in the above mentioned studies.

3.3. Accuracy assessment

Initially, confusion matrices were calculated for each classification result based on the validation data, which consisted of 40 % of the reference data (see 2.2 and Fig. 4). The overall (OA), producer's (PA) and user's accuracies (UA) were calculated along with a confidence interval (CI) of 95 %, therewith taking account of estimation uncertainties (Olofsson et al., 2014). Additionally, the area along with the CIs of each classified salt marsh category was derived. Priorly, the results needed to be masked by the field-mapped salt marsh extent to exclude non-salt marsh pixels.

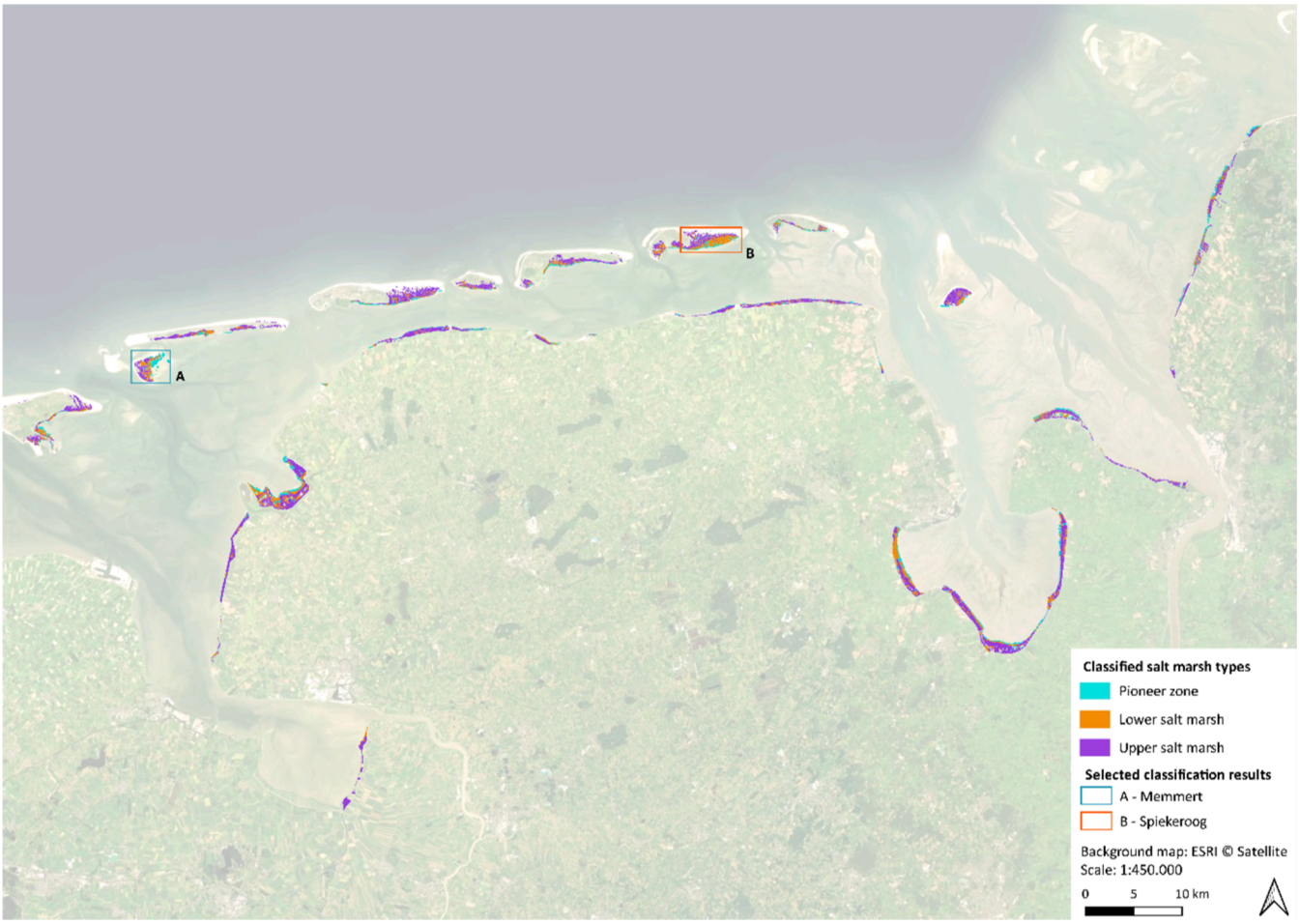

Fig. 5. Classification result of Sentinel-2.

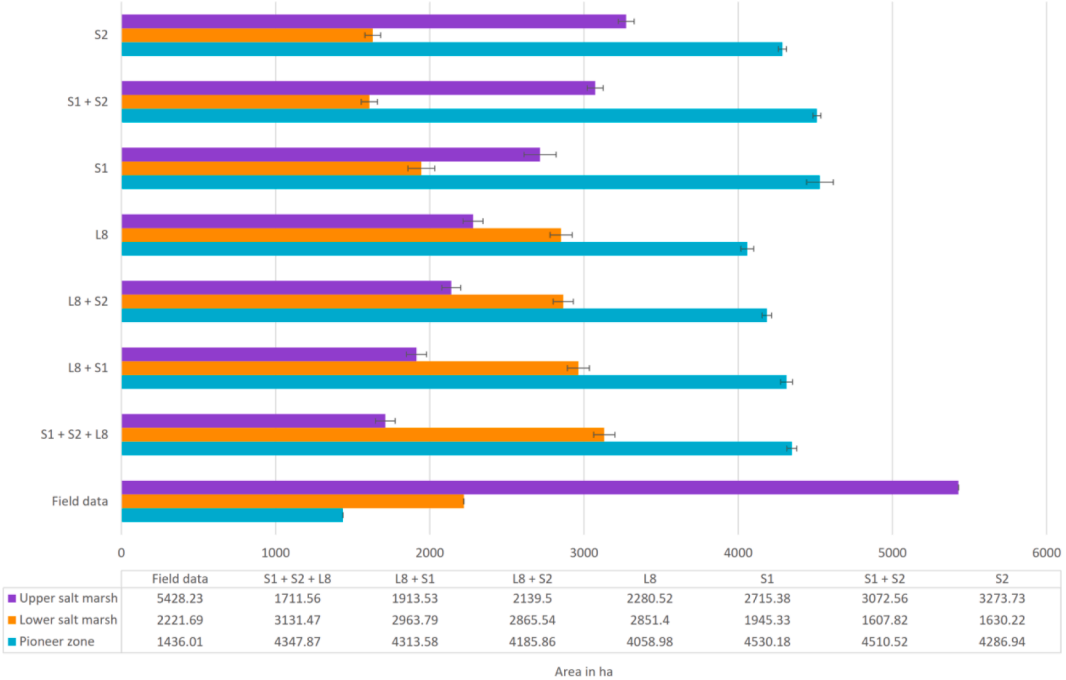

	Field data	S1 + S2 + L8	L8 + S1	L8 + S2	L8	S1	S1 + S2	S2
Upper salt marsh	5428.23	1711.56	1913.53	2139.5	2280.52	2715.38	3072.56	3273.73
Lower salt marsh	2221.69	3131.47	2963.79	2865.54	2851.4	1945.33	1607.82	1630.22
Pioneer zone	1436.01	4347.87	4313.58	4185.86	4058.98	4530.18	4510.52	4286.94

Fig. 6. Predicted salt marsh area in ha.

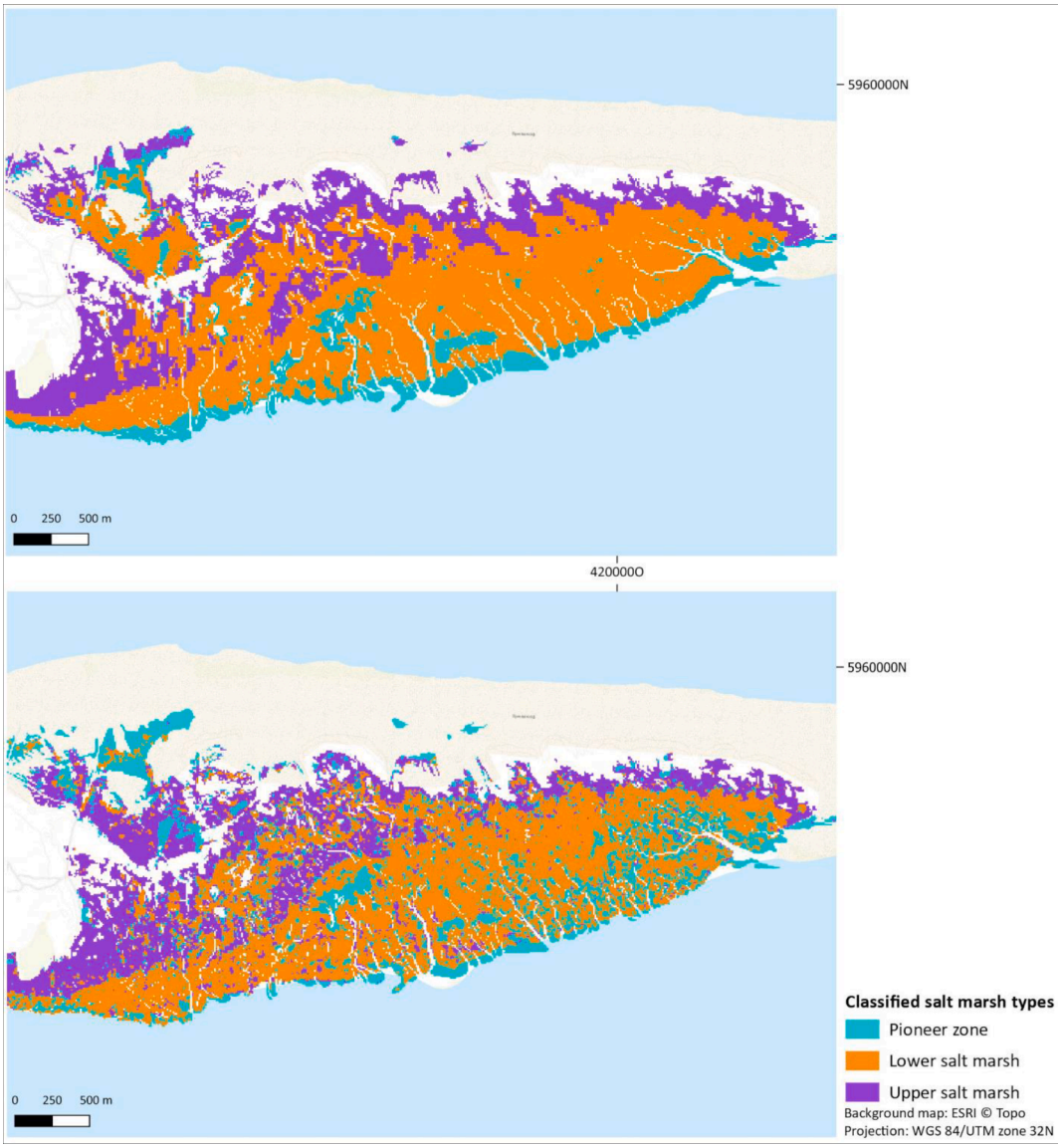

Fig. 7. Classification results of S2 (upper map) and S1 (lower map) for the eastern part of Spiekeroog (rectangle B of map in Fig. 5).

4. Results

4.1. Visual interpretation

The S2 classification agreed well to NLWKN's field data. Misclassifications mainly occured at the boundaries of the salt marsh categories. In comparison, the S1 classification contained a lot of small misclassified areas, occurring in all salt marsh categories. The upper salt marsh was overestimated and confused with both other classes. The central areas were mainly mapped correctly. The result of S1 and S2 combined showed a better classification than S1 alone as less speckle-like areas were mapped. However, the lower salt marsh was more overestimated than by S2 alone. L8 yielded to a larger overestimation of the lower salt marsh compared to S2. L8 combined with S2 featured misclassifications between the lower and upper salt marsh. Nevertheless, the classification performed better than only using L8 and yielded a worse result compared to the classification based on S2 alone. Similarly, the fusion of L8 and S1 as well as the fusion of all three datasets led to higher accuracies than only using mono-sensor data. Generally, lower salt marshes were overestimated in every classification and upper salt marshes were often classified as lower marshes towards the inland.

4.2. Random Forest classification of mono-sensor datasets

The best classification result was obtained with S2: the OA achieved 90.31 ± 0.59 % (Table 3). The UA and PA achieved 90 – 97 % for the pioneer zone and the upper salt marsh. In comparison, the lower salt marshes' PA and UA achieved 70.31 ± 2.50 % and 78.36 ± 1.46 %, respectively. The result of the S2 classification is shown in Fig. 5. Detailed results are given for the isles Memmert and Spiekeroog in Figs. 7 – 8. The S1 classification achieved the lowest OA with 63.08 ± 1.16 %. Regarding the single classes, the PA of the pioneer zone achieved 86.04 ± 0.69 % and an UA of 64.99 ± 1.65 %. The PA and UA of the lower salt marsh, however, achieved 28.02 ± 1.40 % and 44.63 ± 1.53 %, respectively, and the PA and UA of the upper salt marsh 49.88 ± 1.60 % and 68.68 ± 1.81 %, respectively. Only using L8 achieved an OA of 81.57 ± 0.79 %. The UA and PA of the upper salt marsh achieved the highest accuracy with 95.09 ± 0.76 % and 79.63 ± 1.37 %, respectively. The PA and UA of the lower salt marshes achieved 75.39 ± 1.41 % and 69.40 ± 1.62 %, respectively. The PA and the UA of the pioneer zone achieved 87.0 ± 0.89 % and 84.41 ± 1.19 %, respectively.

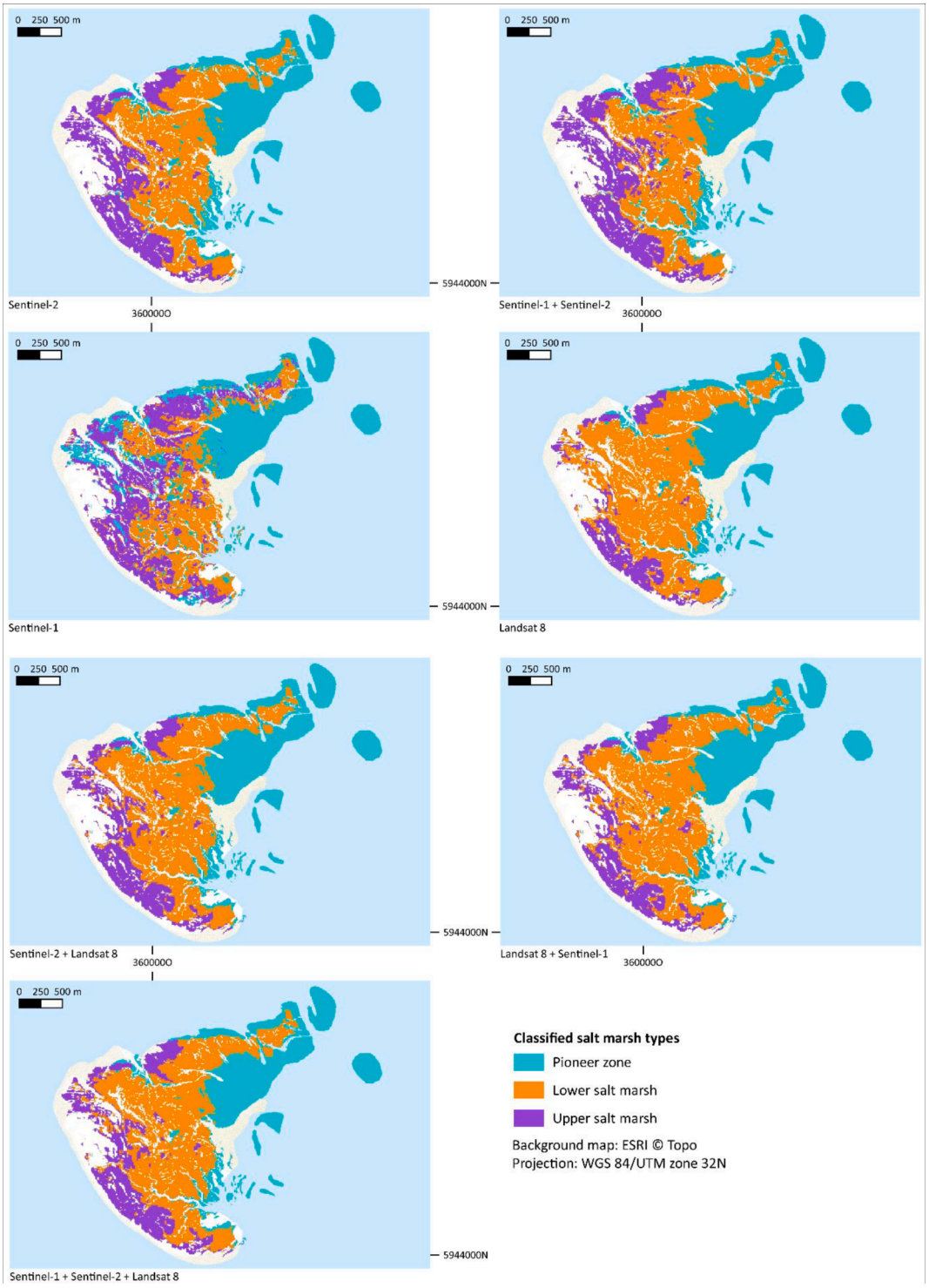

Fig. 8. Classification results for Memmert (rectangle A of map in Fig. 5).

4.3. Random Forest classification of multi-sensor datasets

S2 combined with SAR data achieved similar results to only using S2: the OA of the combination was 90.18 ± 0.60 %, which was slightly worse than S2 alone. However, with respect to the PAs and UAs of the three classes, S1 helped to better map the pioneer zone with the PA achieving 93.21 ± 0.51 % compared to 92.71 ± 0.57 % of S2 and the UA achieving 90.83 ± 0.99 % compared to 90.35 ± 1.00 % of S2. Nevertheless, the individual accuracies of the lower and upper salt marshes decreased by approx. 1 – 2 %. The OA of the combined classification of S2 and L8 achieved 86.10 ± 0.71 %. This was a decrease in accuracy of ca. 4 % compared to only using S2. L8 did not add value to the mapping accuracy of the pioneer zone. Improvements were achieved for the lower and upper salt marshes with PAs of 80.58 ± 1.35 % and 89.67 ± 1.18 % and UAs of 76.81 ± 1.52 % and 96.65 ± 0.61 %, respectively. Compared to the L8 classification setup, the fusion of L8 and S1 led to minor improvements. The OA achieved 82.98 ± 0.78 %. The PA of the pioneer zone achieved 87.29 ± 0.87 % and the UA achieved 86.57 ± 1.13 %. Contrary, the lower salt marshes were mapped with lower accuracies: the PA achieved 78.58 ± 1.38 %, the UA achieved 72.29 ± 1.58 %. The

upper salt marshes were mapped with slightly better accuracies with the PA achieving 80.08 ± 1.55 % and the UA achieving 94.60 ± 0.78 %. The fusion of all datasets (L8, S1 and S2) yielded similar accuracies as the combination of the optical datasets. The OA achieved 85.53 ± 0.75 %. The PA of the pioneer zone achieved 87.41 ± 0.90 % and the UA 88.06 ± 1.08 %. The PA of the lower salt marsh achieved 82.51 ± 1.28 % and the UA 77.33 ± 1.50 %. Lastly, the PA of the upper salt marshes achieved 86.29 ± 1.55 % and the UA 96.31 ± 0.64 %.

4.4. Salt marsh extent

NLWKN mapped an area of 1347.01 ha for the pioneer zone, 2122.42 ha of lower and 4823.26 ha of upper salt marshes in the field, which was used as comparative measurement to the area estimation. The area of the pioneer zone estimated based on Sentinel-2 achieved 4286.94 ± 51.22 ha (Fig. 6). The area of the lower salt marsh achieved 1630.22 ± 51.22 ha and the area of the upper salt marsh 3273.73 ± 26.43 ha. The lower salt marsh estimated based on L8 achieved 2851.4 ± 71.58 ha and the upper salt marsh 2280.52 ± 41.59 ha. The estimation of the pioneer zone achieved an area of 4058.98 ± 64.44 ha. Using S1, the mapped pioneer zone was 4530.18 ± 103.91 ha, the lower salt marsh achieved 1945.33 ± 86.61 ha and the upper salt marsh 2715.38 ± 86.9 ha.

The pioneer zone mapped by the combination of S1 and S2 achieved 4510.52 ± 51.87 ha. The area of lower salt marsh was 1607.82 ± 52.74 ha and the upper salt marsh area 3072.56 ± 25.46 ha. The pioneer zone mapped by the combination of S1 and L8 achieved 4313.58 ± 65.12 ha, the lower salt marsh 2963.79 ± 71.65 ha and the upper salt marsh 1913.53 ± 38.91 ha. The pioneer zone mapped by the combination of both optical sensors, L8 and S2, achieved 4185.86 ± 60.85 ha, the lower salt marshes 2865.54 ± 65.3 ha and the upper salt marshes 2054.85 ± 40.96 ha. The pioneer zone mapped with the S1, S2 and L8 fused datasets achieved 4347.87 ± 64.19 ha, the lower salt marshes 3131.47 ± 68.98 ha and upper salt marshes 1711.56 ± 32.19 ha.

5. Discussion

5.1. Suitability of freely available satellite imagery for salt marsh classification

Our major objective was to assess the general quality of salt marsh mapping using freely available satellite imagery. Overall, the chosen satellite imagery and the proposed strategy are very well suited for mapping the main salt marsh categories. Comparing the different classification results, which were based on the different datasets, it can be assessed that the classification with S2 led to the highest OA. In comparison, the OA of the L8 classification decreased by 8.74 %. The L8 data was resampled to 10 m using the nearest neighbour method, therewith retaining the original reflectance values, while matching the higher spatial resolution of S2 and thereby preserving the higher spectral information. From this, we conclude that the high spatial and temporal resolution of S2 are of great importance. Misclassifications occurring at the boundaries between two classes could result from twofold types of mixed pixels: on the one hand, they exist due to spectral mixing caused by the spatial resolution. Especially L8 with its spatial resolution of 30 m showed more frequent misclassifications at the boundaries compared to S2. On the other hand, mixed pixels in time can exist: The (spectral-)temporal metrics were calculated over a period of three years by assuming no change during this time. However, changes may have occurred, especially at the boundaries between two salt marsh categories, as this is the region with a high chance of change. This assumption could also explain the high confusions between the classes in general. For future applications of our approach, we suggest calculating the metrics over one year to exclude changes in salt marsh types from one year to another and only including the vegetation period to concentrate on phenological characteristics. As the reference data of this study was collected over three years, we chose to calculate the metrics over the same period, ensuring sufficient training data. Aside from mixed pixels, misclassifications of small areas could also appear due to common vegetation species among the superior salt marsh categories. To account for this, we propose to include a fine grid digital elevation model and information on the flooding frequency, as this additional information could assist in differentiating between the superior salt marsh categories. Moreover, the occurring plant species in the salt marshes bloom at different points in time. By calculating spectral-temporal metrics over a period of three years and per salt marsh class instead of plant communities, individual characteristics of the species may not be captured. Thus, we suggest to investigate the potential of S2 for mapping salt marshes at species level, especially for large, consistent areas.

Compared to the results of the (fused) multispectral data, the classification based on the S1 dataset shows that SAR could also be used to map superior salt marsh categories, although the OA was notably lower. When multispectral data is limited due to cloud cover, SAR temporal metrics could also be used as was successfully done by Hu et al. (2021), who achieved an OA of 87.86 %. Regarding the estimated extents of each salt marsh type, the estimated area occupied by lower salt marshes was the closest to the field-mapped area. However, the pioneer zone and the upper salt marsh were over- and underestimated, respectively (see Fig. 6). Frequent misclassifications occured in the lower salt marshes, especially in the areas of tidal creeks. Dependent on the water level within the tide, the SAR signal can be very contrasting. As we did not include water level information, these areas might be captured indistinctly by the SAR temporal metrics.

Besides, there was a substantial amount of misclassifications, which can be seen in the map (Fig. 7, lower map) and the confusion matrix (Table A3 in the appendix). This is in line with other studies. Zhang et al. (2021) also found that a salt marsh classification based on S1 resulted in the worst classification accuracy compared to the optical and SAR fused and the optical datasets (OAs of 92.4 % and 86.36 %, respectively). Compared to Hu et al. (2021), who achieved an OA of 87.86 % in mapping salt marsh species in China using annual S1 metrics and DT classifiers, our SAR based classification performed weaker. Our approach to focus on the superior salt marsh categories might be unsuitable for SAR data. The species of each salt marsh category could have similar roughness properties and thus, the SAR signal is not suitable for differentiation on the chosen classification level.

The classification using L8 shows the general capability of distinguishing between the classes (Table A4, appendix). Zeng et al. (2022) proofed the suitability of L8 in mapping salt marsh species using temporal composites in a phenology-based vegetation index classification and achieved OAs of 80 – 90 %, which is in line with our OA of 81.57 % for the L8 classification of superior salt marsh categories. We assume that a L8 classification on species level would perform weaker, as in our study site more than ten species occur very small-scale spreaded. In general, the salt marsh classification of L8 achieved adequate results and could be used for a historical (change) analysis of salt marsh categories. When considering the estimated areas of the salt marsh types (see Fig. 8), S2 was much closer to the originally mapped salt marshes (except for the overestimated pioneer zone) compared to L8. Sun et al. (2018) conducted a multi-temporal classification of salt marsh vegetation communities using flexible monthly NDVI Time-Series based on Landsat 5 and 7 using DTs. Based on this approach, they achieved an OA of 89.8 % compared to using single multi-spectral images (avg. OA of 79.1 %), which yielded better results than our classification (ca. – 8 %) using a multi-temporal and multi-feature approach. A possible reason for the quite large difference in these results could be the fact that the spectral-temporal metrics were calculated over a period of three years, which might miss to depict relevant information that in turn a dense time-series, like Sun et al. (2018) used, does. Laengner et al. (2019) used Landsat 5 data to map the salt marshes extent across Europe using GEE and an unsupervised, manual DT. The mapping for all four time steps resulted in OAs between 93 and 95 %. Compared to our L8 based classification, they achieved a classification more than 10 % more accurate. The authors included information on the water level, which could

explain the higher accuracies. However, from the analysts perspective, Laengner et al.'s classification approach has some limitations, as manual thresholds are needed for the used indices and thus might not be directly transferable. One of three aims of this study was to investigate if L8 complements a S2 times series in case of limited data availability due to cloud cover. Our results do not allow making a point in this relation and we suggest to further investigate this by simulating limited S2 data. This approach would be helpful, when considering to calculate the spectral-temporal metrics year-wise. The comparison of the classification results based on the optical datasets, S2 and L8, shows that the higher temporal and spatial resolution of S2 plays an important role in mapping the three superior salt marsh categories. Additionally, if sufficient S2 scenes are available, we recommend using them solely as L8 does not contribute to the classification in this case.

The estimated area proportions (Fig. 6) showed that the pioneer zone was overestimated by all classification approaches. We assume that it is very challenging to define the boundary between the pioneer zone and the lower salt marsh in the field as well as with satellite data. The lower salt marsh is still flooded almost as often as the pioneer zone, which could result in similar spectral reflectance in optical and backscatter in SAR data. To take account of this issue, we suggest to either exclude flooded pixels or include a water-sensitive index.

5.2. Added value of SAR data

Another objective of this study was to assess the suitability of combining multispectral and SAR data for mapping salt marshes on category level. In our case, under consideration of the OA and the CIs, the fused S1 and S2 classification was as good as the S2 classification. This is in contrast to the findings of Zhang et al. (2021), who achieved the best result with the combination of S1 and S2 (OA of 92.4 %). Nevertheless, they investigated three different salt marsh species and included field spectral data of different growth states of the species. We assume that S1 would improve the result when conducting the classification on species level as well. However, in the case of limited S2 data due to cloud cover, S1 could increase the classification accuracy, which needs further investigations. Concerning the estimated salt marsh extents, S1 worsened the proportions compared to the originally mapped extent. The fusion of S1 and L8 shows that SAR had minimal contribution to the classification accuracy. The classification result of all combined datasets led to the same conclusion. Initially, we expected S1 data to add value to the classification as was shown in many other vegetation and especially salt marsh mapping studies (Joshi et al., 2016; Muro et al., 2020; Zhang et al., 2021). S1 created an added value in the wetland mapping conducted by Muro et al. (2020). Their study addressed the challenge of limited S2 data availability due to cloud cover, as they found half as much S2 than S1 data. In our case, SAR data might not add valuable information as the roughness characteristics of the superior salt marsh classes are not distinctly distinguishable. Moreover, frequent flooding of the pioneer zone and partly the lower salt marsh can hamper SAR to differentiate the salt marsh types. Nevertheless, S1 could be useful if the availability of optical data is constrained by cloud cover. Our study proofs that the spectral-temporal information of Sentinel-2 is of greater importance than the roughness and moisture captured by SAR.

5.3. Recommendations for operational salt marsh monitoring

In view of operational monitoring as obliged to *Natura 2000*, our study provides a simple methodological approach: the calculation of (spectral-)temporal metrics is easy to automise and allows the constant inclusion of the latest satellite images. A RF classifier is straightforward to parametrise, performs well on small amounts of training data and is easily conveyed to other investigation periods and other study areas. The use of freely available multispectral remote sensing data cannot replace the field mapping. Our study shows that superior salt marsh categories (pioneer zone, lower and upper salt marsh) can be mapped with a very high OA of 90 %. Thus, this approach can support the field mapping, e.g., by conducting a change analysis based on yearly S2 spectral-temporal metrics, allowing for prioritizing areas for field mapping at species level.

To ameliorate our approach, we suggest to filter the satellite imagery according to the tides and thus to exclude flooded areas. To address this, we suggest eliminating flooded pixels based on the TMII proposed by O'Connell et al. (2017). Furthermore, limiting the investigated period to the vegetation period (e.g., March – September) could further enhance the classification accuracy by precluding observations that contain irrelevant information for the differentiation of the salt marsh categories.

6. Conclusions

To summarize, all free available satellite products used in this study are suitable to map superior salt marsh categories at the coast of Lower Saxony (Germany) using (spectral-)temporal metrics and a basic Random Forest classifier with very good to satisfying accuracies. Sentinel-2 yielded with over 90 % the best result and is the prefered choice, provided a sufficient amount of cloud-free data is available. If this it not the case, Sentinel-2 could be fused with either Sentinel-1 or Landsat 8. Our approach can be implemented to support the planning of the field mapping by identifying and hence prioritizing areas of occurred change. Moreover, the capability of Landsat 8 in mapping salt marshes is adequate for conducting a change analysis over a long period.

Funding

This research did not receive any specific grant from funding agencies in the public, commercial, or not-for-profit sectors.

Submission declaration

The work presented in the manuscript has not been published before and is not under consideration for publication elsewhere. The publication is approved by all authors and will not be published in the same form after acceptance for publication.

Author contributions

Kim-Jana Stückemann designed the study, processed and analyzed the data, interpreted the results, and wrote the manuscript.

Björn Waske was involved in this process, e.g. by supporting the study design and data analysis as well as reviewing and editing the manuscript.

Declaration of Competing Interest

The authors declare that they have no known competing financial interests or personal relationships that could have appeared to influence the work reported in this paper.

Data availability

The authors do not have permission to share data.

Acknowledgements

The authors thank Lower Saxony Water Management, Coastal Defense and Nature Conservation Agency (*German:* „Niedersächsischer Landesbetrieb für Wasserwirtschaft, Küsten- und Naturschutz", NLWKN) for providing the dataset "Basiserfassung der FFH-Gebiete in Niedersachsen – Auszug Wattenmeer" (Eds. NLWKN 2015-2017) of Lower Saxony's FFH region Wadden Sea, containing the salt marsh biotopes and species mapping. The authors particularly thank their colleagues from the working group Remote Sensing and Digital Image Analysis of the Institute of Computer Science, Osnabrück University, for their support and feedback on this study.

Appendix

See Table A1, Table A2, Table A3, Table A4, Table A5, Table A6, Table A7.

Table A1
Confusion matrix of the Sentinel-2 classification. (PZ: Pioneer zone, LSM: Lower salt marsh, USM: Upper salt marsh).

		Classification		
		PZ	LSM	USM
Reference	PZ	3006	321	0
	LSM	467	2404	197
	USM	92	61	3250

Table A2
Confusion matrix of the fused Sentinel-1 and Sentinel-2 classification.

		Classification		
		PZ	LSM	USM
Reference	PZ	2982	301	0
	LSM	503	2412	225
	USM	80	73	3222

Table A3
Confusion matrix of the Sentinel-1 classification.

		Classification		
		PZ	LSM	USM
Reference	PZ	2098	587	543
	LSM	1071	1801	1163
	USM	396	398	1741

Table A4
Confusion matrix of the Landsat 8 classification.

		Classification		
		PZ	LSM	USM
Reference	PZ	3010	555	1
	LSM	484	2148	463
	USM	71	83	2983

Table A5
Confusion matrix of the fused Landsat 8 and Sentinel-2 classification.

		Classification		
		PZ	LSM	USM
Reference	PZ	3052	426	0
	LSM	472	2289	219
	USM	41	71	3228

Table A6
Confusion matrix of the fused Landsat 8 and Sentinel-1 classification.

		Classification		
		PZ	LSM	USM
Reference	PZ	3004	466	0
	LSM	487	2218	363
	USM	74	102	3084

Table A7
Confusion matrix of the fused Sentinel-1, Sentinel-2 and Landsat 8 classification.

		Classification		
		PZ	LSM	USM
Reference	PZ	3046	413	0
	LSM	466	2302	209
	USM	53	71	3238

References

Belgiu, M., Drăguţ, L., 2016. Random forest in remote sensing: A review of applications and future directions. ISPRS J. Photogramm.Remote Sens. 114, 24–31. https://doi.org/10.1016/j.isprsjprs.2016.01.011.

Breiman, L., 2001. Random Forests. Machine Learning 45, 5–32. https://doi.org/10.1023/A:1010933404324.

Bruzzone, L., Marconcini, M., Wegmuller, U., Wiesmann, A., 2004. An advanced system for the automatic classification of multitemporal SAR images. IEEE Trans. Geosci. Remote Sens. 42 (6), 1321–1334. https://doi.org/10.1109/TGRS.2004.826821.

Bundesamt für Seeschifffahrt und Hydrographie. 2022. Wasserstandsvorhersage Nordsee: Wasserstandsvorhersage des BSH. Accessed via: https://www.bsh.de/DE/DATEN/Vorhersagen/Wasserstand_Nordsee/ wasserstand_nordsee_node.html;jsessionid=7719BC5B9BFFFB5E94D1BC7CFD0ED04E.live21321 (26th April, 2022).

Campbell, A.D., Wang, Y., Wu, C., 2020. Salt marsh monitoring along the mid-Atlantic coast by Google Earth Engine enabled time series. PLOS ONE 15 (2), e0229605. https://doi.org/10.1371/journal.pone.0229605.

Cao, F., Tzortziou, M., 2021. Capturing dissolved organic carbon dynamics with Landsat-8 and Sentinel-2 in tidally influenced wetland-estuarine systems. Sci. Total Environ. 777, 145910 https://doi.org/10.1016/j.scitotenv.2021.145910.

Carrasco, L., O'Neil, A., Morton, R., Rowland, C., 2019. Evaluating Combinations of Temporally Aggregated Sentinel-1, Sentinel-2 and Landsat 8 for Land Cover Mapping with Google Earth Engine. Remote Sens. 11 (3), 288. https://doi.org/10.3390/rs11030288.

Dara, A., Baumann, M., Freitag, M., Hölzel, N., Hostert, P., Kamp, J., Müller, D., Prishchepov, A.V., Kuemmerle, T., 2020. Annual Landsat time series reveal post-Soviet changes in grazing pressure. Remote Sens. Environ. 239, 111667 https://doi.org/10.1016/j.rse.2020.111667.

Davy, A., Bakker, J., Figueroa, M.E., 2009. Human modification of European salt marshes. In: Silliman, B.R., Grosholz, T., Bertness, M.D. (Eds.), HumAn ImpActs on SAlt MArshes: A GlobAl Perspective. University of California Press, Berkeley, California, USA, pp. 311–336.

ESA. 2021. Technical Guides: Sentinel-2 MSI. https://sentinels.copernicus.eu/web/sentinel/technical-guides/sentinel-2-msi/level-2a/algorithm (26th April, 2022).

Esselink, P., Petersen, J., Arens, S., Bakker, J.P., Bunje, J., Dijkema, K.S., Hecker, N., Hellwig, U., Jensen, A.-V., Kers, A.S., Körber, P., Lammerts, E.J., Stock, M., Veeneklaas, R.M., Vreeken, M., Wolters, M. 2009. Salt Marshes. Thematic Report No. 8. In: Marencic, H., de Vlas, J. (Eds): Quality Status Report 2009. Wadden Sea Ecosystem No. 25. Common Wadden Sea Secretariat, Trilateral Monitoring and Assessment Group, Wilhelmshaven, Germany, pp. 54.

Esselink, P., van Duin, W.E., Bunje, J., Cremer, J., Folmer, E.O., Frikke, J., Glahn, M., de Groot, A.V., Hecker, N., Hellwig, U., Jensen, K., Körber, P., Petersen, J., Stock, M. 2019. Salt Marshes. In: Wadden Sea Quality Status Report 2017. Accessed via: qsr.waddensea-worldheritage.org/reports/salt-marshes (28th April 2022).

European Commission: Directorate-General for Environment: Mézard, N., Sundseth, K., Wegefelt, S. 2008. Natura 2000: protecting Europe's biodiversity. Doi: 10.2779/45963.

Gao, B.C., 1996. NDWI—a normalized difference water index for remote sensing of vegetation liquid water from space. Remote Sens. Environ. 58, 257–266. https://doi.org/10.1016/S0034-4257(96)00067-3.

Gedan, K.B., Kirwan, M.L., Wolanski, E., Barbier, E.B., Silliman, B.R., 2011. The present and future role of coastal wetland vegetation in protecting shorelines: answering recent challenges to the paradigm. Clim. Change 106, 7–29. https://doi.org/10.1007/s10584-010-0003-7.

Harris, C.R., Millman, K.J., van der Walt, S.J., Gommers, R., Virtanen, P., Cournapeau, D., Wieser, E., Taylor, J., Berg, S., Smith, N.J., Kern, R., Picus, M., Hoyer, S., van Kerkwijk, M.H., Brett, M., Haldane, A., del Río, J.F., Wiebe, M., Peterson, P., Gérard-Marchant, P., Sheppard, K., Reddy, T., Weckesser, W., Abbasi, H., Gohlke, C., Oliphant, T.E., 2020. Array programming with NumPy. Nature 585 (7825), 357–362.

Hu, Y., Tian, B.o., Yuan, L., Li, X., Huang, Y., Shi, R., Jiang, X., Wang, L., Sun, C., 2021. Mapping coastal salt marshes in China using time series of Sentinel-1 SAR. ISPRS J. Photogramm.Remote Sens. 173, 122–134.

Ienco, D., Interdonato, R., Gaetano, R., Minh, D.H.T., 2019. Combining Sentinel-1 and Sentinel-2 Satellite Image Time Series for land cover mapping via a multi-source deep learning architecture. ISPRS J. Photogramm.Remote Sens. 158, 11–22. https://doi.org/10.1016/j.isprsjprs.2019.09.016.

Joshi, N., Baumann, M., Ehammer, A., Fensholt, R., Grogan, K., Hostert, P., Jepsen, M.R., Kuemmerle, T., Meyfroidt, P., Mitchard, E.T.A., Reiche, J., Ryan, C.M., Waske, B., 2016. A Review of the Application of Optical and Radar Remote Sensing Data Fusion to Land Use Mapping and Monitoring. Remote Sens. 8 (1), 70. https://doi.org/10.3390/rs8010070.

Laengner, M.L., Siteur, K., van der Wal, D., 2019. Trends in the Seaward Extent of Saltmarshes across Europe from Long-Term Satellite Data. Remote Sens. 11 (14), 1653. https://doi.org/10.3390/rs11141653.

Li, H., Wang, C., Cui, Y., Hodgson, M., 2021. Mapping salt marsh along coastal South Carolina using U-Net. ISPRS J. Photogramm. 179, 121–132.

Mandanici, E., Bitelli, G., 2016. Preliminary Comparison of Sentinel-2 and Landsat 8 Imagery for a Combined Use. Remote Sens. 8, 1014. https://doi.org/10.3390/rs8121014.

McFeeters, S.K., 1996. The use of normalized difference water index (NDWI) in the delineation of open water features. Int. J. Remote Sens. 17, 1425–1432. https://doi.org/10.1080/01431169608948714.

Müller, H., Rufin, P., Griffiths, P., Barros Siqueira, A.J., Hostert, P., 2015. Mining dense Landsat time series for separating cropland and pasture in a heterogeneous Brazilian

savanna landscape. Remote Sens. Environ. 156, 490–499. https://doi.org/10.1016/j.rse.2014.10.014.

Müller, G., Stelzer, K., Smollich, S., Gade, M., Adolph, W., Melchionna, S., Kemmen, L., Geißler, J., Millat, G., Reimers, H.G., Kohlus, J., Eskildsen, K., 2016. Remotely sensing the German Wadden Sea - a new approach to address national and international environmental legislation. Environ. Monit. Assess. 188, 595. https://doi.org/10.1007/s10661-016-5591-x.

Muro, J., Varea, A., Strauch, A., Guelmami, A., Fitoka, E., Thonfeld, F., Diekkrüger, B., Waske, B., 2020. Multitemporal optical and radar metrics for wetland mapping at national level in Albania. Heliyon 6 (8), e04496.

O'Connell, J.L., Mishra, D.R., Cotten, D.L., Wang, L., Alber, M., 2017. The Tidal Marsh Inundation Index (TMII): An inundation filter to flag flooded pixels and improve MODIS tidal marsh vegetation time-series analysis. Remote Sens. Environ. 201, 34–46. https://doi.org/10.1016/j.rse.2017.08.008.

Olofsson, P., Foody, G.M., Herold, M., Stehman, S.V., Woodcock, C.E., Wulder, M.A., 2014. Good practices for estimating area and assessing accuracy of land change. Remote Sens. Environ. 148, 42–57. https://doi.org/10.1016/j.rse.2014.02.015.

Pedregosa, F., Varoquaux, G., Gramfort, A., Michel, V., Thirion, B., Grisel, O., Blondel, M., Louppe, G., Prettenhofer, P., Weiss, R.J., Vanderplas, J., Passos, A., Cournapeau, D., Brucher, M., Perrot, M., Duchesnay, E., 2011. Scikit-learn: Machine Learning in Python. J. Mach. Learn. Res. 12, 2825–2830.

Pflugmacher, D., Rabe, A., Peters, M., Hostert, P., 2019. Mapping pan-European land cover using Lansat spectral-temporal metrics and the European LUCAS survey. Remote Sens. Environ. 221, 583–595. https://doi.org/10.1016/j.rse.2018.12.001.

Potapov, P.V., Turubanova, S.A., Tyukavina, A., Krylov, A.M., McCarty, J.L., Radeloff, V. C., Hansen, M.C., 2015. Eastern Europe's forest cover dynamics from 1985 to 2012 quantified from the full Landsat archive. Remote Sens. Environ. 159, 28–43. https://doi.org/10.1016/j.rse.2014.11.027.

Rüetschi, M., Schaepman, M.E., Small, D., 2018. Using Multitemporal Sentinel-1 C-band Backscatter to Monitor Phenology and Classify Deciduous and Coniferous Forests in Northern Switzerland. Remote Sens. 10 (1), 55. https://doi.org/10.3390/rs10010055.

Rufin, P., Müller, H., Pflugmacher, D., Hostert, P., 2015. Land use intensity trajectories on Amazonian pastures derived from Landsat time series. Int. J. Appl. Earth Obs. Geoinf. 41, 1–10. https://doi.org/10.1016/j.jag.2015.04.010.

Schuerch, M., Spencer, T., Temmerman, S., Kirwan, M.L., Wolff, C., Lincke, D., McOwen, C.J., Pickering, M.D., Reef, R., Vafeidis, A.T., Hinkel, J., Nicholls, R.J., Brown, S., 2018. Future response of global coastal wetlands to sea-level rise. Nature 561, 231–234.

Common Wadden Sea Secretariat (CWSS), Wilhelmshaven, Germany; Trilateral Salt Marsh and Dunes Expert Group. 2017. TMAP-Typology of Coastal Vegetation in the Wadden Sea Area. Version 1.0.4. Accessed via: www.waddensea-secretariat.org/saltmarsh (5th April, 2022).

Silliman, B.R., Grosholz, T., Bertness, M.D., 2009. Salt marshes under global siege. In: Silliman, B.R., Grosholz, T., Bertness, M.D. (Eds.), HumAn ImpActs on SAlt MArshes: A GlobAl Perspective. University of California Press, Berkeley, California, USA, pp. 103–114.

Sun, C., Fagherazzi, S., Liu, Y., 2018. Classification mapping of salt marsh vegetation by flexible monthly NDVI time-series using Landsat imgery. Estuar. 61–80. https://doi.org/10.1016/j.ecss.2018.08.007.

Sun, C., Li, J., Liu, Y., Liu, Y., Liu, R., 2021. Plant species classification in salt marshes using phenological parameters derived from Sentinel-2 pixel-differential time-series. Remote Sens. Environ. 256, 112320 https://doi.org/10.1016/j.rse.2021.112320.

Tucker, C.J., 1979. Red and photographic infrared linear combinations for monitoring vegetation. Remote Sens. Environ. 8(2), 9, 127–150. https://doi.org/10.1016/0034-4257(79)90013-0.

Van Rossum, G., Drake, F.L., 2009. Python 3 Reference Manual. CreateSpace, Scotts Valley, CA.

Veloso, A., Mermoz, S., Bouvet, A., Le Toan, T., Planells, M., Dejoux, J.-F., Ceschia, E., 2017. Understanding the temporal behavior of crops using Sentinel-1 and Sentinel-2-like data for agricultural applications. Remote Sens. Environ. 199, 415–426. https://doi.org/10.1016/j.rse.2017.07.015.

Wang, Q., Blackburn, G.A., Onojeghuo, A.O., Dash, J., Zhou, L., Zhang, Y., Atkinson, P. M., 2017. Fusion of Landsat 8 OLI and Sentinel-2 MSI Data. IEEE Trans. Geosci. Remote Sens. 55 (7), 3885–3899. https://doi.org/10.1109/TGRS.2017.2683444.

Waske, B., Benediktsson, J.A., 2007. Fusion of support vector machines for classification of multisensor data. IEEE Trans. Geosci. Remote Sens. 45 (12), 3858–3866. https://doi.org/10.1109/TGRS.2007.898446.

Waske, B., van der Linden, S., Oldenburg, C., Jakimow, B., Rabe, A., Hostert, P., 2012. imageRF - A user-oriented implementation for remote sensing image analysis with Random Forests. Environ. Model. Softw. 35, 192–193. https://doi.org/10.1016/j.envsoft.2012.01.014.

Zeng, J., Sun, Y., Cao, P., Wang, H., 2022. A phenology-based vegetation index classification (PVC) algorithm for coastal salt marshes using Landsat 8 images. Int. J. Appl. Earth Obs. Geoinf. 110, 102776 https://doi.org/10.1016/j.jag.2022.102776.

Zhang, C., Gong, Z., Qiu, H., Zhang, Y., Zhou, D., 2021. Mapping typical salt-marsh species in the Yellow River Delta wetland supported by temporal-spatial-spectral multidimensional features. Sci. Tot. Environ. 783, 147061 https://doi.org/10.1016/j.scitotenv.2021.147061.